Combination of MRI-Guided High-Intensity Focused Ultrasound and Bioluminescent Biological Systems to Assess Thermal Therapies for Tumor and Tumor Microenvironment

Pauline Jeanjean, Dounia El Hamrani, Coralie Genevois, Bruno Quesson, Franck Couillaud

Combination of MRI-guided High Intensity Focused Ultrasound and Bioluminescent Biological Systems to Assess Thermal Therapies for Tumor and Tumor Microenvironment

*Pauline Jeanjean [1§], Dounia El Hamrani [2,3§], Coralie Genevois [1,4], Bruno Quesson [2.3 *], Franck Couillaud [1 *]*

1- IMOTION (Molecular imaging and innovative therapies in oncology), EA 7435, Bordeaux University, Bordeaux, France
2- IHU LIRYC (Electrophysiology and Heart Modeling Institute), Hopital Xavier Arnozan, Pessac, France
3- Centre de recherche Cardio-Thoracique de Bordeaux, INSERM U1045, Bordeaux, France
4- VIVOPTIC-TBM Core, Bordeaux University, CNRS UMS 3427, INSERM US 005, Bordeaux, France

* Corresponding authors: Franck.Couillaud@u-bordeaux.fr & Bruno.Quesson@u-bordeaux.fr
§ Co-authors

Keywords: MRgHIFU, cancer therapies, bioluminescence imaging, mouse model, tumor microenvironment, Hsp

Abstract: This work presents an integrated technology for assessing *in vivo* anti-cancer treatments in mice, based on various heating conditions. Bioluminescence imaging (BLI) was used to assess the physiological response of tumor and tumor microenvironment (TME) to heat treatment induced by magnetic resonance-guided high-intensity focused ultrasound (MRgHIFU). Transgenic tumor cells and mouse models with either constitutive or thermo-induced luciferase expressions were combined to monitor cell viability and heat-induced processes in the tumor and TME. BLI performed after MRgHIFU heating shows that a moderate increase in temperature (45°C) over 5 min can be exploited to promote heat-activable treatments in the tumor and its TME, without inducing direct cell death. A higher temperature rise over a shorter exposure time can induce cell death in the tumor, as revealed by a reduction in the BLI signal after treatment. Under these conditions, BLI also revealed that the TME can be stimulated by heat without inducing necrosis. These integrated technologies and models are useful to assess, *in vivo* in mice, the efficacy of various anticancer strategies exploiting local heat deposition by noninvasive MRgHIFU, including those combining tumor ablation with local drug administration using thermosensitive nanovehicles.

1. Introduction

Solid tumors are complex structures composed of tumor cells, and the tumor microenvironment (TME) containing extracellular matrix and various noncancerous cells, including fibroblasts, vascular endothelial cells and immune cells.[1] The TME plays a major role in tumor evolution and also modulates the tumor response to therapies.[2] To improve the efficiency of tumor treatments, some therapeutic strategies not only target cancer cells, but also address the TME to combine therapies to kill tumor cells with strategies stimulating the TME to induce anticancer effects.

Thermal therapies are part of the anticancer arsenal. They are increasingly used as they provide similar efficacy to surgery, but with reduced side effects and a shorter recovery time for the patient. During such treatment, the effective temperature change within the pathological

and surrounding healthy tissues results from an equilibrium between heat deposition and dissipation. These parameters remain difficult to assess a priori and can vary due to a number of biological parameters (e.g. tissue structure and heterogeneity, vascularization, perfusion rate).

Several sources of energy can induce a local temperature increase in biological tissue, such as microwaves,[3–5] lasers,[6,7] radiofrequency,[8,9] high-intensity focused ultrasound (HIFU) [10–12] and magnetic hyperthermia.[13–15] However, HIFU has drawn considerable interest since it is noninvasive and can exploit both thermal and mechanical effects. Moreover, it can be combined with online magnetic resonance thermometry (MR thermometry) to assess temperature change in space and time during the procedure. In addition, using a regulation algorithm, HIFU energy deposition can be adjusted dynamically and automatically from iterative MR temperature images to force the temperature at the desired location to follow a predefined time-temperature profile.[11,12,16,17]

MR-guided HIFU (MRgHIFU) can provide a non-invasive conformal treatment and is thus gaining interest for clinical treatments, such as for uterine fibroid,[18] essential tremor,[19,20] painful bone metastasis,[21] prostate cancer [22–24]and breast cancer.[25,26] The current preferred use of MRgHIFU for cancer therapies is to induce thermal coagulation necrosis of the tumor. However, as the aforementioned therapies based only on thermal tumor cell ablation through high temperature increases (typically exceeding 60 °C) have often failed in complete patient cure and led to local recurrence or metastasis, thermal ablative therapies have been coupled with local treatments such as radiotherapy[27] and systemic chemotherapy[28,29] to improve overall treatment efficacy, but still with limited results. To further improve the efficiency of thermal-based tumor treatments, therapeutic strategies have been proposed exploiting mild hyperthermia to favor local drug release from thermosensitive nanoparticles,[30–34] enhanced macromolecule delivery[35] and thermo-induced gene or miRNA expression by tumor cells [36–38] or tumor-associated macrophages (TAM).[39] For instance, synergy effects of ablative techniques and immunotherapies are currently being explored clinically and are referred to as an abscopal effect.[40–43] The challenge is to kill most of the tumor cells without completely impairing TME viability. This requires precise control of heating conditions, which can be achieved noninvasively by MRgHIFU technology. In clinical practice, tumor regression or progression after thermotherapies is assessed by measuring tumor dimensions by CT or MR imaging [44–47], and could be combined with PET imaging to evaluate metabolic activity[48]. The proof of concept of innovative therapies based on thermal treatment is usually performed first on rodents. As a complement to anatomical imaging provided by MRI or CT, BLI could be used as a convenient alternative to PET imaging, as BLI can provide assessment of tumor metabolism with high sensitivity and is further accessible to many sophisticated transgenic models [16,37,39,49–51].

This work aims to present *in vivo* proof of concept of such a dual approach in mice, illustrating the potential of local control of heat deposition to exploit different and concomitant thermal effects targeting both tumor cells and the TME. To achieve this goal, several heating conditions corresponding to mild-hyperthermia or thermo-coagulation were applied to wild-type and transgenic mice bearing different genetically-modified subcutaneous tumors. Cancer cell lines were modified to follow different luciferases showing changes in tumor cell viability (by constitutive-luciferase expression) or non-lethal thermal stimulation (by heat-induced luciferase expression using a heat shock protein (Hsp) promoter) *in vivo* by BLI. Transgenic mice modified for thermo-induced luciferase expression were also used for tumor implantation to follow the TME response to mild hyperthermia. Thus, using non-invasive and controlled MRgHIFU heating combined with BLI, we provided *in vivo* images of mice, illustrating locally-heated tumors combined with heat-activated TME.

2. Results

2.1. Generation and characterization of a thermosensitive tumor cell line

A murine prostate cancer cell line (RM1) was generated for thermo-induced firefly luciferase (Fluc) expression under transcriptional control of the Hsp70 promoter. The resulting RM1-Hsp70-Fluc cells were characterized for response to heat shock using a water bath for heating and measurement of luciferase activity on cell lysate 6 hours after the heat shock. These results show that a water bath heating at 45 °C for 5 minutes (min) provides the optimal conditions to favor Hsp70 promoter activation and Fluc expression in this tumor cell line (**Figure S1)**. After heating at 48 °C for 5 min, no Fluc activity was further observed.

2.2. Tumor mild hyperthermia induced by MRgHIFU heating

According to the previous results, the same range of targeted conditions (43; 44; 45 and 47 °C / 5 min) were selected to induce MRgHIFU heating on mice bearing RM1-Hsp70-Fluc tumors (N = 13). A predefined time-temperature profile served as an input to a feedback algorithm that automatically adjusted the delivered HIFU power from online MR thermometry. A good correspondence between targeted and experimental temperature values was observed (**Figure S2**), with residual oscillations on the resulting temperature curves. Since the amplitude of such oscillations (standard deviation +/ 1°C) is in a similar range to the different temperature increases (43 to 47°C), the data analysis was performed on temporally and spatially averaged temperature around the hottest pixel (see Material and Methods section and **Figure S3**). The hottest value in the resulting spatiotemporally filtered temperature map was reported and analyzed regarding BLI signals. Depending on the measured heating conditions, different BLI pattern could be observed as illustrated by the typical example in **Figure 1**. For low heating conditions (42.7 ± 0.7 °C / 5 min; N = 4; **Figure 1.A**), either a small increase in BLI signal was observed only at the HIFU entrance point (N = 3) or no increase (N = 1) in BLI signal was observed. These results suggest that for a treatment duration of 5 min, temperatures lower than 43 °C are not sufficient to induce a detectable activation of the Hsp70 promoter in the whole tumor. For heating conditions around 45 °C for 5 min (44.8 ± 0.3 °C / 5 min; N = 4; **Figure 1.B**), the BLI signal was covering the tumor area and was quite spatially uniform. For higher heating conditions, (46.5 ± 0.7 °C / 5 min; N = 5; **Figure 1.C**) spatial distribution of the BLI signal appeared heterogeneous within the tumor, with a peripheral bioluminescent area (due to effective Hsp70 promoter activation) and a central point without a BLI signal. The absence of signal in the central point might be attributed to inefficient local activation of the Hsp70 promoter or more likely to local cell death induced by MRgHIFU overheating. Taken together, the results confirmed that thermo-dependent expression of Fluc could be non-invasively induced by mild hyperthermia (i.e. temperature ranging from 43 to 46°C for a duration of 5 min) in tumor.

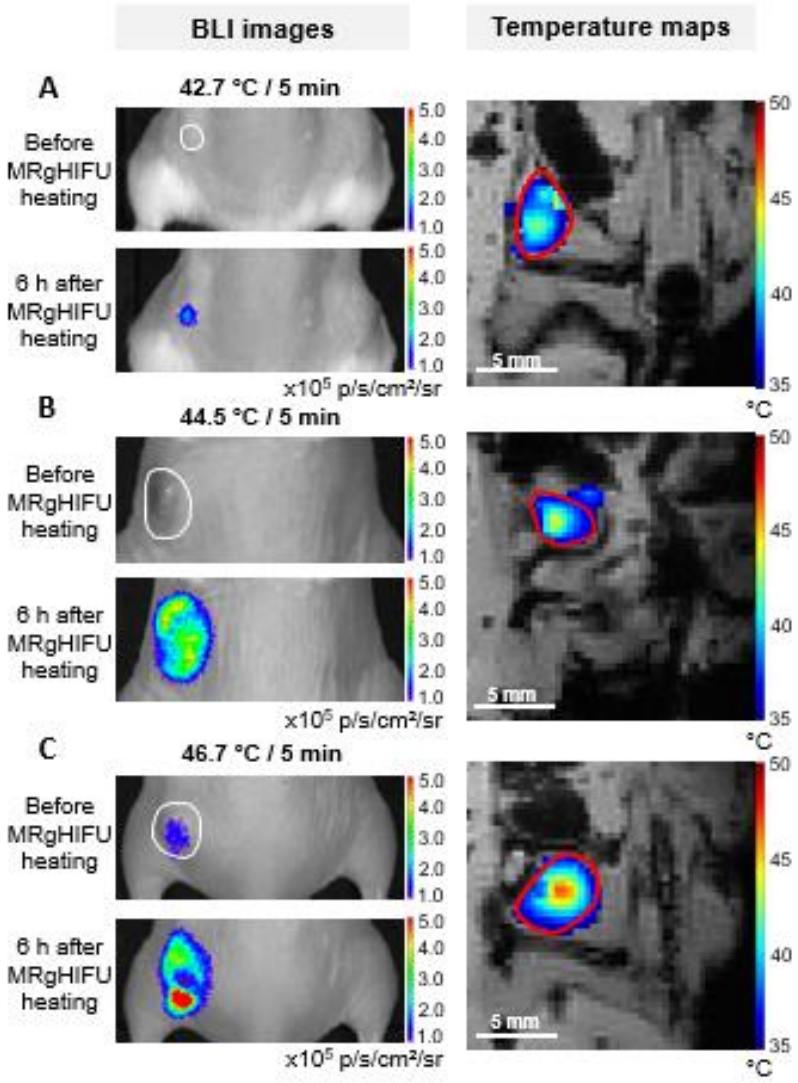

Figure 1. Changes in BLI signal after tumor mild hyperthermia induced by MRgHIFU heating *in vivo*. Wild-type mice bearing RM1 tumors with thermo-inducible Fluc expression (RM1-Hsp70-Fluc). Typical images of BLI signal and corresponding temperature maps illustrating 3 different heating conditions 42.7 °C / 5 min (**A**), 44.5 °C / 5 min (**B**) and 46.7 °C / 5 min (**C**). BLI signals were measured before and 6 hours after MRgHIFU application. The white line on the BLI image delimits tumor edge. Temperature maps represent the average temperature of MRgHIFU heating and the mean temperature of the surroundings voxels. The red line in the temperature map delimits tumor edge defined on MRI images prior to heating.

2.3. Tumor thermal ablation induced by MRgHIFU heating

In a second batch of experiments, different temperature-time profiles were applied to induce coagulation necrosis. Thus, a range of high temperatures was applied for a short duration (between 55 and 60 °C for 1 min). To highlight the effects of thermal ablation on tumor growth and tumor cell viability, tumors from RM1 cells with a constitutive expression of Fluc (RM1-CMV-Fluc) were implanted on WT C57bl6 albino mice (N = 9). Analysis was performed by using the measured temperatures and two different groups were formed depending on temperature ranges. Typical examples of each group are shown in **Figure 2** with BLI images, temperature maps and the corresponding BLI profile. For tumors heated with temperatures

ranging from 48.7 to 54.3 °C (52.2 ± 2.4 °C / 1 min; N=4; **Figure 2.A**), the BLI profile after treatment had the same "bell-shaped" distribution as before MRgHIFU application, but with a higher intensity that highlights persistence of tumor growth.

For tumors heated with measured temperatures ranging from 54.9 to 64.2 °C, two different patterns of BLI profiles were observed, depending on the heated zone location, either central or eccentric (60.7 ± 3.7 °C / 1 min; N=5; **Figure 2.B&C**). For the central heating zone, as illustrated in **Figure 2.B**, the BLI profile after treatment exhibited the same "bell-shaped" distribution as before heating but with significantly lower intensity, illustrating a decrease in tumor cell viability. For the eccentric heating zone, (**Figure 2.C**)**,** the BLI profile shapes were very different before and after heating, showing some tumor areas with a decrease in BLI signal after heating, corresponding to the location of the heated zone, and tumor areas with an increased BLI signal, corresponding to non-heated areas and continued growth of the tumor.

In this experiment, skin burn spots were observed surrounding the entrance point of the HIFU beam for 4 mice. No burn spots were observed on the ventral side of mice.

These results confirm that when heat deposition higher than 54 °C for 1 min is sufficient to induce coagulation necrosis, a decrease in BLI is observed in the heated zone.

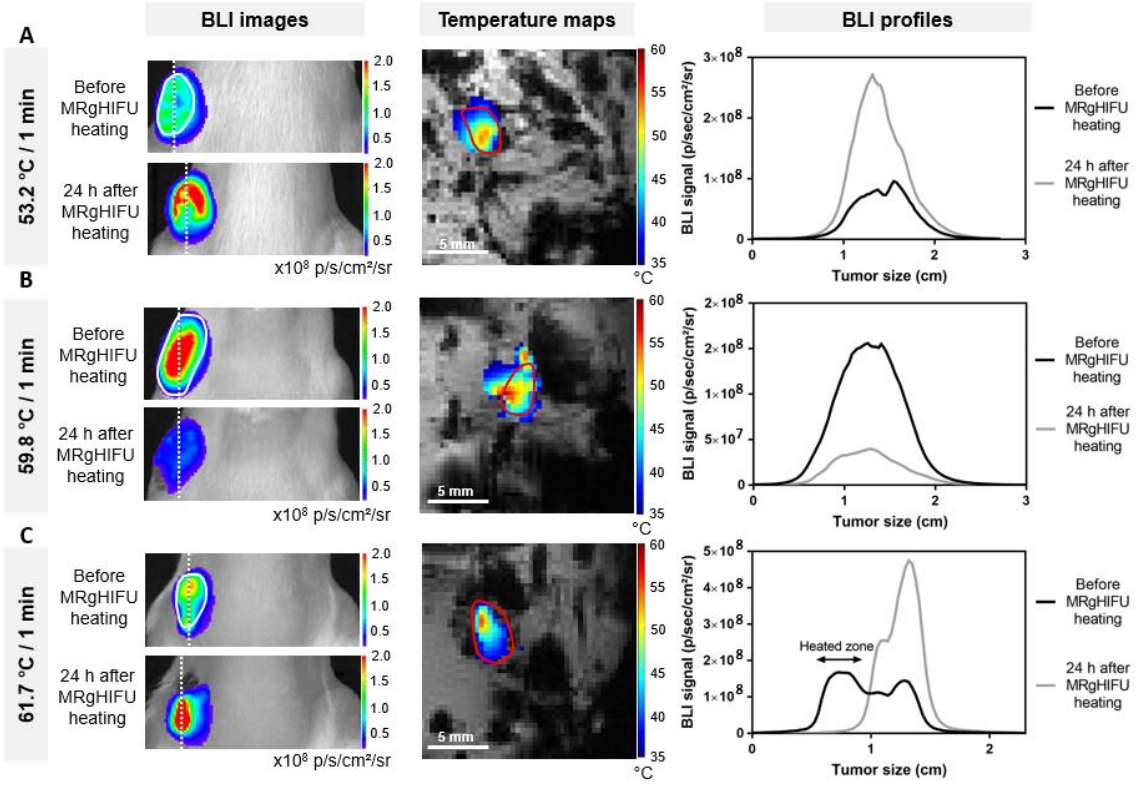

Figure 2. Changes in BLI signal after tumor thermal ablation induced by MRgHIFU heating *in vivo*. Wild type mice bearing RM1 tumors with constitutive expression of Fluc (RM1-CMV-Fluc). BLI images, temperature maps and BLI profiles of 3 mice treated by MRgHIFU heating at 53.2 °C / 1 min (**A**), 59.8 °C / 1 min (**B**) and 61.7 °C / 1 min (**C**). BLI profiles represent the BLI signal profile along the dotted white line before (black curve) and after (grey curve) MRgHIFU heating. In BLI images, the white line delimits the tumor edge and the dotted white line represents the craniocaudal axis including the maximum intensity pixel used to perform the BLI profile. Temperature maps represent the average temperature of

MRgHIFU heating and the mean temperature of the surroundings voxels. The red line in the temperature map delimits tumor edge defined on MRI images prior to heating.

2.4. Mild hyperthermia induced by MRgHIFU in both tumor and TME

In this experiment, two different luciferases under transcriptional control of the Hsp promoter were used to discriminate signals from tumor cells and TME. RM1 cells expressing Nanoluciferase (Nluc) (RM1-Hsp70-Nluc) were grown on transgenic mice expressing Fluc (Hsp-Fluc). Light resulting from Nluc activity could not be discriminated from light resulting from Fluc activity but as Fluc and Nluc require different substrates (D-luciferin and Furimazin, respectively), enzymatic activities were measured sequentially in 2 separate BLI sessions (at 6 hours and 24 hours, respectively). Heat-induced expression controlled by Hsp promoter are transient [52]. Maximum Fluc activity in the transgenic mouse occurred 6 hours after heat shock [16,52]. To delay thermo-induced expression of Nluc in RM1 cells, Nluc were encoded as a fusion iRFP/2A/Nluc protein containing a protease 2A cleavage site. Translation process of the fusion protein was increased thus modifying the time course of heat-induced Nluc activity. Using the fusion precursor, the maximum Nluc activity occurred at 24 hours after heating instead of 6 hours when Nluc is encoded alone. Thus, the thermo-induced signals from TME (Fluc) and tumor cells (Nluc) could be easily discriminated.

Several targeted hyperthermia conditions using an MRgHIFU setup were applied from 45.8 to 46.9 °C (46.3 ± 0.5 °C / 5 min; N = 7). As shown in one typical example in **Figure 3**, the heating procedure led to an increase in BLI signal from both the tumor and TME. As shown by the temperature map, the heat delivered at the focal point and its diffusion all around the focal point enabled mild hyperthermia to be exploited in both the tumor and TME (see **Figure S4** for supplementary mice).

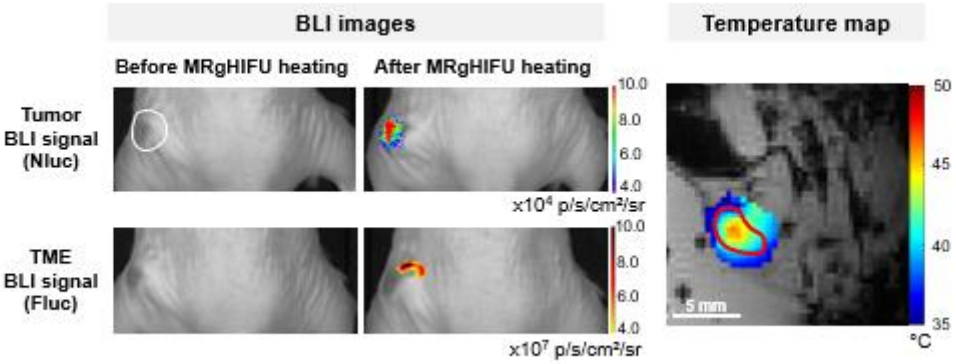

Figure 3. Changes in BLI signal after mild hyperthermia in tumor and TME induced by MRgHIFU heating. Transgenic mice with thermo-inducible Fluc expression (Hsp-Fluc) bearing RM1 tumors with thermo-inducible expression of Nluc (RM1-Hsp70-Nluc). BLI images of tumor and TME, before and after MRgHIFU heating and temperature map of a mouse treated at 46.8 °C for 5 min. Fluc and Nluc BLI images after MRgHIFU heating were captured at 6 and 24 h, respectively. Temperature maps represent the average temperature of MRgHIFU heating and the mean temperature of the surroundings voxels. The white line on the BLI image delimits tumor edge. The red line in the temperature map delimits tumor edge defined on MRI images prior to heating.

2.5. Tumor thermal ablation by MRgHIFU and TME activation assessment by BLI

Effects of tumor thermal ablation by MRgHIFU on TME were investigated. For this, RM1 tumors exhibiting constitutive expression of Nluc (RM1-CMV-Nluc) were grown on thermosensitive mice (Hsp-Fluc) (N = 10). Before heating, BLI revealed a strong signal from constitutive Nluc expression by tumor cells, but no signal from Fluc by the TME. A thermo-coagulation heating protocol (temperature range from 54 to 62 °C for 1 min) was applied to tumors using the MRgHIFU setup. In **Figure 4.A**, a representative result of a HIFU heating spot applied near the center of the tumor is presented. As a result, an overall decrease in the Nluc signal in the tumor was measured 24 hours after heating (58.2 ± 4.0 °C / 1 min; N = 4), indicative of tumor necrosis. **Figure 4.B** shows a representative result of a HIFU heating spot positioned laterally to the tumor (58.2 ± 3.2 °C / 1 min; N = 6). In this situation, two zones can be observed in Nluc BLI, a sharp decrease in the heated zone and a remaining ring of light in the non-heated zone showing insufficient thermal energy deposition to create coagulation. Regardless of the heating location within the tumor, the BLI signal (Hsp-Fluc) from the tissues surrounding the tumor (TME) showed a "ring-shaped" photon distribution resulting from heat diffusion from the heating zone (**Figure 4.A&B**), indicative of sufficient thermal stress to activate the Hsp-dependent transcription of FLuc, while remaining nondestructive for the tissue (see **Figure S5** for supplementary mice**)**. Altogether, these results showed that MRgHIFU heating can lead to targeted thermal ablation of the tumor combined with non-destructive heating of the TME using mild hyperthermia.

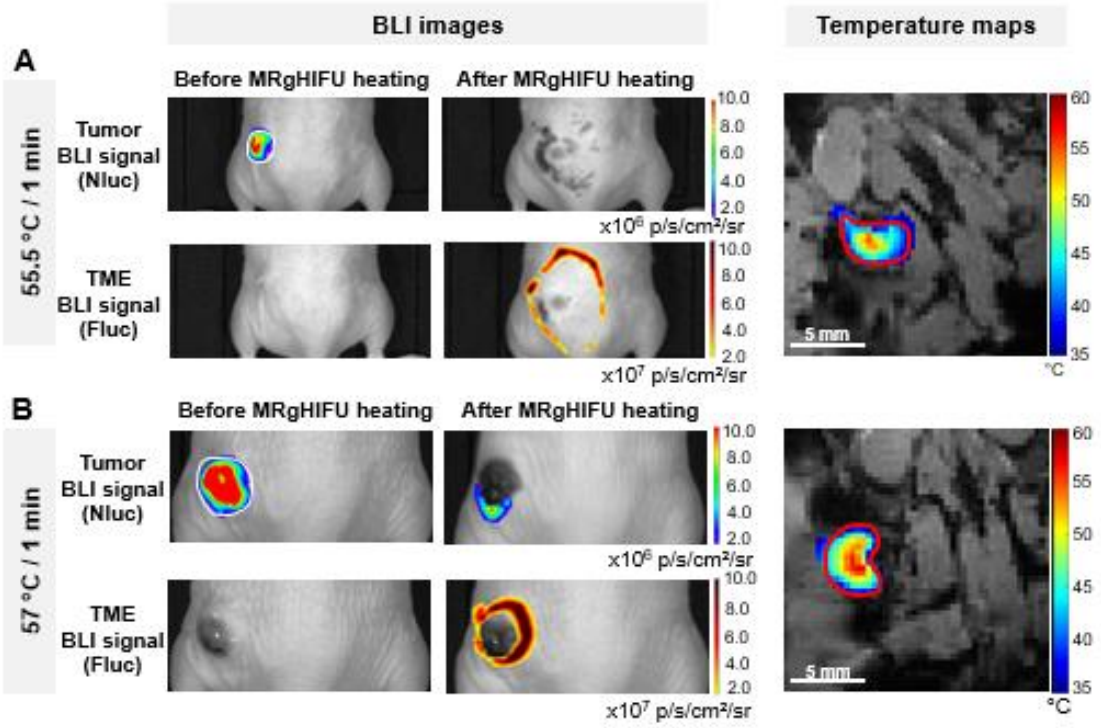

Figure 4. Tumor thermal ablation by MRgHIFU heating and BLI assessment TME activation by BLI. Transgenic mice with thermo-inducible Fluc expression (Hsp-Fluc) bearing RM1 tumors with constitutive expression of Nluc (RM1-CMV-Nluc). BLI images before and after MRgHIFU treatment and temperature maps of 2 mice treated at 55.5 °C / 1 min (**A**) and 57 °C / 1 min (**B**). The BLI images after MRgHIFU heating of the TME and the tumor were captured 6 and 24 hours respectively after the heating treatment. The white line on the BLI image delimits apparent tumor edge. Temperature maps represent the average temperature of MRgHIFU heating and the mean temperature of the surroundings voxels. The red line in the temperature map delimits tumor edge defined on MRI images prior to heating.

2.6. Heating effects on tumor cells

Cell damage induced by MRgHIFU treatments was evaluated by optical microscopy on HES-stained tumor slices 24 hours after heating (**Figure 5**). It enabled the nucleus to be identified in purple (hematoxylin staining), cytoplasm in pink (eosin staining) and collagen fibers in orange (Saffron staining). Dead-cell areas (white arrows) were characterized by small, dark nuclei resulting from typical staining of chromatin condensation. For non-heated tumors (**Figure 5.A**), only a few small dead-cell areas were observed in large RM1 tumors. For mild hyperthermia treatments, as heating conditions increased, both the size and frequency of cell death areas increased, consistent with BLI data (**Figure 5.B**). In the ablated part of the tumor after severe heating conditions (>53 °C for 1 min), cell death areas represented most of the tumor slice (**Figure 5.C**).

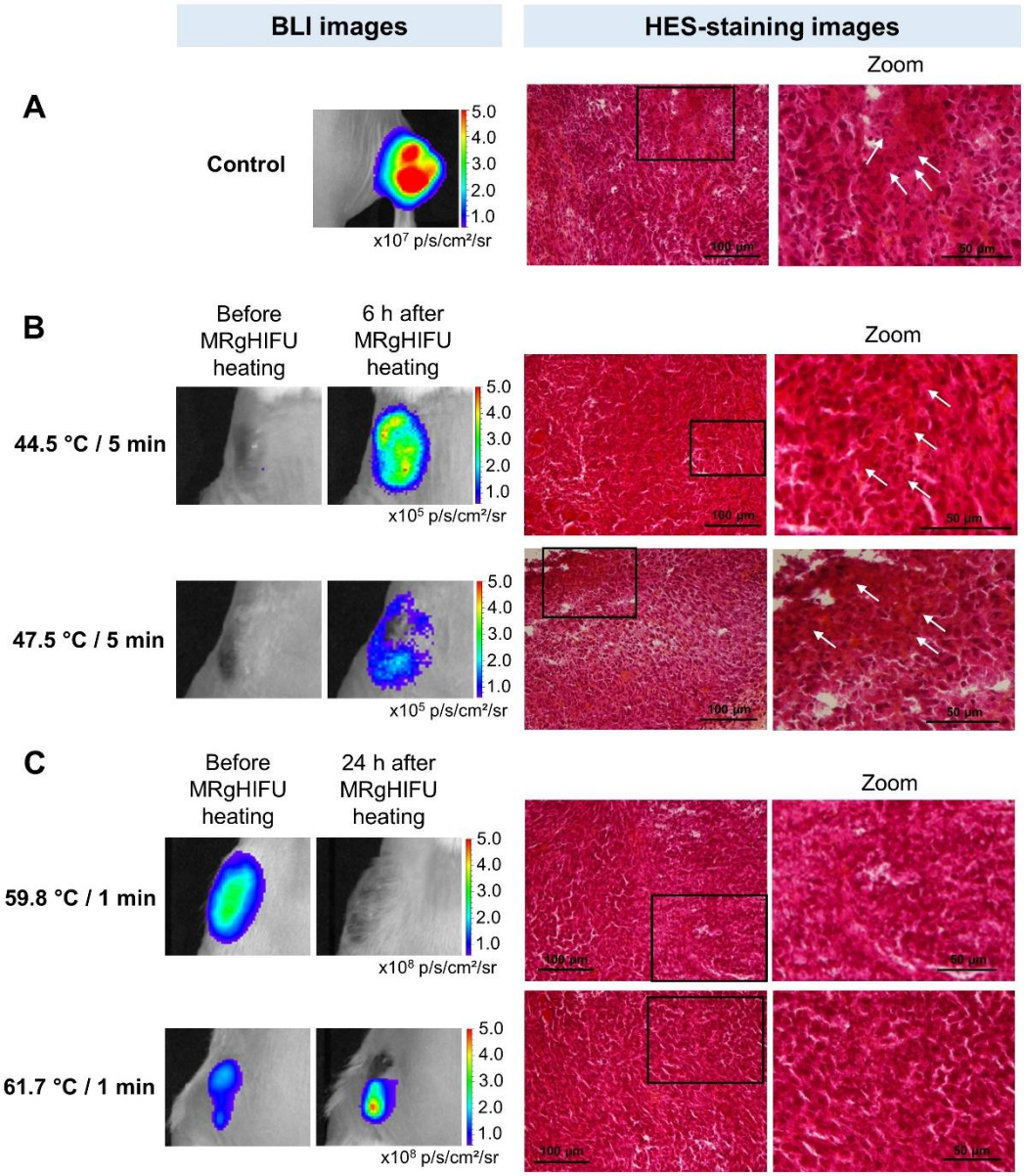

Figure 5. BLI pattern and corresponding HES-stained histology sections of excised tumors after MRgHIFU heating. HES-stained tumor slices with control tumor (RM1-CMV-Fluc tumor) (without MRgHIFU heating) (**A**), RM1-Hsp70-Fluc tumors heated by MRgHIFU at 44.5 or 47.5 °C for 5 min (**B**) and RM1-CMV-Fluc tumors heated by MRgHIFU at 59.8 or 61.7 °C for 1 min (**C**). HES staining enables the nucleus to be identified in purple, cytoplasm

in pink and collagen fibers in orange. For each tumor slice, the part shown in close-up represents the black square insert and white arrows show cell death areas. For each condition, corresponding BLI data were provided for comparison.

3. Discussion

This study shows an original technological approach combining transgenic mice and several tumor cells (expressing luciferase either constitutively or not after a thermal stress), noninvasive and controlled heating by MRgHIFU and BLI to characterize innovative thermotherapies under different modes of operation and to monitor tumor response after treatment. We demonstrate that local controlled heating can be performed, leading to either mild hyperthermia or thermal ablation in tumors and concomitant mild hyperthermia in the TME.

Validation was made possible *in vivo* by BLI using a combination of mice models (including a transgenic mouse with temperature-dependent expression of luciferases) bearing different tumors made of cancer cells exhibiting either constitutive or temperature-inducible luciferase expression. These models allow the physiological impact of the heating conditions applied to the tissue to be seen *in vivo* in 6 or 24 hours. Decreases in BLI signal in tumors with constitutive expression of luciferase are widely used to reveal a decrease in cell viability and a reduction in tumor growth. The appearance of light in tissues (tumor and TME) expressing luciferases under transcriptional control of Hsp promoter shows the physiological response of tissues to mild hyperthermia, a temperature increases sufficient to activate heat-induced physiological processes but not enough to impair cell viability. These models thus provide key animal models to evaluate new therapeutic strategies combining thermal ablation of the tumor and activation of the TME.

The HIFU system used in the present work is dedicated to small animals and the resulting HIFU focal point is thus adapted for heating subcutaneous tumors implanted in mice. In comparison to the literature, the HIFU focal point was similar to other preclinical devices (from 3 to 5 mm in length and 1 mm in width),[16,35,39] but was smaller than clinical devices (from 8 to 15 mm of length and from 3 to 8 mm of width).[53] Moreover, this study was performed with a preclinical high-field MRI scanner dedicated to small animals, which allowed us to achieve a high spatial resolution of MR thermometry (667 x 667 μm^2/pixel) and a high signal-to-noise ratio (~50), with a temporal resolution similar to those reported in the literature (from 1.05 to 3 s).[16,39,54] The target temperature was monitored thanks to a feedback loop implemented for automatic control of HIFU heating within a single voxel. Analysis of MR thermometry images was performed by the individual measurements of the 8 voxels surrounding the reference voxel, which revealed temperature variations among adjacent voxels. Such differences are consistent with the small dimensions of the HIFU spot and may also reflect micro-heterogeneity in tissues relative to ultrasound absorption, heat diffusion, perfusion and potential occurrence of vessels or micro-necrotic areas in the tumor. Consequently, the mean temperature over these 9 voxels (in-plane resolution of the reference voxel and surrounding voxels = 2 x 2 mm^2) was used to characterize temperature change within the region of interest, providing a more representative measure of the temperature changes within the tumor. In our results, the measured temperature was slightly below the target temperature, which was attributed to underachievement of the automatic feedback control algorithm in its current implementation.

Despite similar heating conditions leading to thermal ablation of the tumor by MRgHIFU, *in vivo* BLI revealed different outcomes according to the location of the heating zone within the tumor and therefore the position of the HIFU focal point. Proximity of bones and/or viscera near the tumor prevented precise positioning of the focal point in the center of the tumor. These adjacent structures are composed of heterogeneous media (collagen fibers and

inorganic minerals in bones, gas in the digestive tract) which can result in tissue damage when submitted to the ultrasound beam. Since the objective was to analyze the effect of different time-temperature profiles *in vivo* by BLI, we chose a conservative approach to avoid any sonication toward these critical structures. As a result, no animals experienced adverse effects, except small skin burns at the entrance location of the HIFU beam (in only 4 of the 50 animals included in the MRgHIFU protocol, each of these 4 animals being submitted to a high temperature increase), which can be easily managed for longitudinal studies. In order to induce conformal thermal ablation, it will be necessary to perform sequential changes of the focal point position by mechanical displacements of the transducer (craniocaudal and mediolateral directions) using our setup. Alternatively, 3D electronic deflection of the focal spot to cover the tumor is technically feasible and already available in a number of clinical HIFU systems (i.e. double spiral trajectory) [55,56]. Although a number of tumors were partially heated and resulted in incomplete reduction of BLI and progression of the tumor growth, MR-thermometry data and BLI results were concordant, showing the benefit of the proposed technology and animal/tumor cell lines to evaluate new antitumor strategies. Moreover, histology data on tumors confirmed a high rate of cancer cell death in the targeted area.

The major drawback of systemic anticancer therapies such as chemotherapies is systemic side effects. Local anticancer therapies are expected to limit systemic side effects and are currently based on tumor resection or local treatment with physical processes (thermal and non-thermal effects, including radiotherapy). They are aiming for a complete resection of the tumor (by killing tumor cells), but always face the problems of 3D conformational treatment, margin delimitations and the necessity of preserving healthy adjacent tissues, leading to a crucial choice between therapeutic efficiency and safety. Disseminated tumor cells occurring in the periphery of the tumor are difficult to detect and reach, but are often responsible for local relapses or metastases. By using MRgHIFU heating, we show that it is possible to overcome these limitations by performing TME mild hyperthermia non-invasively. It can be achieved by either controlling moderate heat deposition within the tumor and the surrounding tumor tissue (by MR thermometry feedback), or by combination with thermal ablation of the tumor, which leads to a thermal gradient around the heating point. In this study, the temperature increase within tissues was measured locally by MR thermometry during the heating and the result of the thermal treatment was assessed *in vivo* by BLI, thanks to luciferase expression under transcriptional control of heat shock protein promoter (Hsp70). These complementary approaches allowed the induction of thermo-dependent processes to be evaluated while respecting TME cell viability.

This proof-of-concept study highlighted the advantage of modulating heat deposition by MRgHIFU in order to exploit thermal effects for a concomitant therapy of the tumor and its microenvironment. MRgHIFU can be used as a straightforward therapy by inducing thermal ablation of the tumor, combined with a TME mild hyperthermia at the periphery of the tumor or as a combination of thermo-induced treatments. Anticancer strategies based on heat-induced therapeutic responses have been proposed in the literature, including heat-induced gene or miRNA expression by tumor cells [16,36,57] or by TME.[39] These strategies remain complex and quite far from clinical application, as they also require genetic modifications. The combination of MRgHIFU with thermosensitive nanoparticles loaded with a cytotoxic agent [30–33,58] or enhanced macromolecule delivery [35] could be translated more easily into clinical practice. The combination of controlled MRgHIFU heating and *in vivo* BLI with cutting-edge biological models proposed in this study provides an elegant solution to assess the therapeutic efficacy of these combined strategies.

4. Conclusion

This study showed a controlled spatio-temporal heat treatment by using an MRgHIFU set up on transgenic tumor cell lines and mouse models with constitutive or thermo-induced luciferase expressions. Thereby, it made the proof of concept *in vivo* for several tumor thermo-therapy strategies based on MRgHIHU heating and combining thermo-ablation or mild hyperthermia to target both tumor cells and TME. The physiological response as revealed by BLI in mice is paving the route for new therapeutic strategies alternative to or synergetic to thermo-ablation and based on mild hyperthermia such as drug release from thermo-sensitive nanocarriers, boost of immune response or thermo-modulation of gene expression.

5. Experimental Methods

Mice handling and tumor generation

Animal manipulations were performed in accordance with European directives on the care and use of animals and have been approved by the ethical committee CEEA50 under agreement #11359. The immuno-competent mice were C57bl6 albino (B6N-Tyrc-Brd/BrdCrCrl) mice (8 to 12-week-old). The transgenic thermosensitive mice were immunocompetent C57bl6 (B6N-Tyrc-Brd/BrdCrCrl) Hspa1b-Fluc (+/+) Hsp1b-mPlum (+/+) mice (10 to 27-week-old).[59] Animals were housed at the University facilities and maintained under 12-hour dark/light cycles with water and food provided *ad libitum*. Mice were anesthetized with 1.5 % isoflurane in air (Belmont, Nicholas Piramal Limited, London, UK). For imaging and MRgHIFU applications, mice were shaved with clippers and depilatory cream. Tumors were generated using cells injected subcutaneously on the left flank or the leg (2.10^6 cellules/100 µL of PBS) in anesthetized mice. Tumor growth was monitored by bioluminescence imaging (BLI).

Plasmid construction

The pcDNA5-CMV-iRFP-ires-Nluc vector was obtained by replacing the Fluc sequence from the pcDNA5-CMV-iRFP-ires-Fluc vector [60] by the Nluc sequence from the pNL2.1 vector (Promega, Madison, WI). To obtain the pcDNA5-FRT-Hsp-iRFP-2A-Nluc vector, the CMV promoter from the pcDNA5-CMV-iRFP-ires-Nluc was replaced by the Hsp sequence from the pcDNA3.1-Hsp-FLuc vector [37], and the iRFP stop codon and the ires sequence was replaced by the protease 2A sequence [61].

Cancer cell line generation and culture

Murine prostate cancer cell lines, RM1, provided by Dr T.C. Thompson (Baylor College of Medicine, Houston, TX, USA) were cultured in Dulbecco's modified Eagle's medium (DMEM) (Invitrogen; Carlsbad, CA, USA) supplemented with 1 % of antimycotic-antibiotic mix (PSA, Invitrogen) and 10 % of fetal bovine serum (FBS, Invitrogen). They were maintained in a humidified 5 % CO_2 incubator at 37 °C.

Generation of the RM1-CMV-Fluc cell line was described previously.[62]The RM1-Hsp70-FLuc cell line was obtained by transfection with a pcDNA3.1-Hsp-FLuc vector [37] using Lipofectamine reagent (Invitrogen) and selected by Neomycin (750 µg/mL, Euromedex, Souffelweyersheim, France). RM1-FRT-Hsp-iRFP-2A-Nluc (called RM1-Hsp70-Nluc) and RM1-FRT-CMV-iRFP-ires-Nluc (called RM1-CMV-Nluc) cell lines were obtained by using the Flp-in system (Invitrogen) in 2 steps: (i) a RM1 recombinant clone containing Flp Recombination Target (FRT) sites was first selected with zeocin (350 µg/mL, Invitrogen); (ii) it was co-transfected with pOG44 vector encoding Flp recombinase and either pcDNA5-FRT-

Hsp-iRFP-2A-Nluc or pcDNA5-FRT-CMV-iRFP-ires-Nluc vectors using lipofectamine reagent. Cell lines were then selected with Hygromycine B (700 µg/mL, Euromedex).

MRgHIFU heating procedure

For MRgHIFU heating, anesthetized mice (1.5 % isoflurane in air, 0.5 L/min) placed on a circulating warm waterbed were monitored for body temperature using a rectal probe (**Figure 6**). A pressure sensor was used to monitor the respiration cycle (SA Instrument, Stony Brook, USA). Aqueous gel was applied on the HIFU transducer and the mouse hind leg to obtain a homogeneous medium for ultrasound propagation. A block of agarose gel was placed at the exit of the ultrasound beams from the tissues to prevent untargeted heating of tissues at this interface.[63]

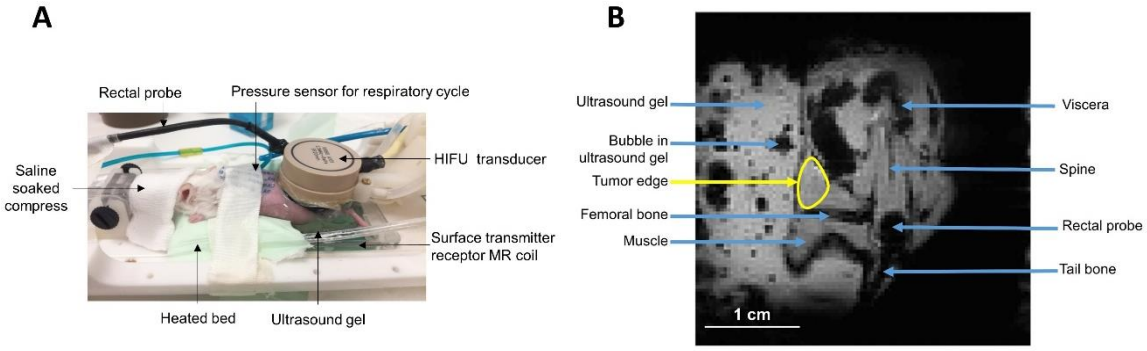

Figure 6. Mouse positioning in the MRgHIFU setup and organs identification on MR images. (A) The anesthetized mouse was laid on a heated bed with a saline soaked compress on its face to prevent dry eyes. A rectal probe and a pressure sensor were used to monitor body temperature and respiratory frequency, respectively. Ultrasound gel was placed throughout the ultrasound beam. (B) Coronal magnitude image of the MR-thermometry sequence showing different organs of the animal and ultrasound gel. The tumor edge is surrounded in yellow.

MRgHIFU experiments were performed on a 9.4 T MRI scanner (Bruker Biospin 9.4/30, Ettlingen, Germany) equipped with a shielded gradient insert (114 mm inner diameter, maximum gradient strength 660 T/m). The hind leg of the mouse was positioned over a surface transmitter receptor coil incorporated into the bed.

The HIFU transducer contained 8 elements (Imasonic, Besancon, France) operated at 2.4 MHz. Its aperture and natural focal length were 25 mm and 20 mm, respectively, resulting in a focal point size of 5 mm in length and 1 mm in width. The positioning of the transducer relative to the tumor in the craniocaudal and mediolateral directions was based on scout view MR-images acquired prior to HIFU energy delivery. Particular care was taken to avoid sonicating in bones and/or viscera, to avoid tissue damage in these areas. The scout MR-images were also used to define the tumor edge on temperature maps.

For MR thermometry, a fast low-angle shot (FLASH) sequence was used with the following parameters: 3 slices orthogonal to ultrasound beam axis and centered on the focal point, TR = 25 ms, TE = 5 ms, 96 x 96 matrix size, field of view = 64 x 64 mm, in-plane resolution = 667 x 667 µm^2/pixel, slice thickness = 1 mm, flip angle = 10°, bandwidth = 50 kHz, 2.4 s temporal resolution per stack. Temperature images were processed on the fly using the water proton resonance frequency shift (PRF)[64–66] technique and were displayed online with Thermoguide software (Image Guided Therapy, Pessac, France) which also regulated (automatic feedback from predefined temperature-time profiles) the tumor temperature in a single pixel by automatically adjusting the output power of the HIFU generator at each new incoming temperature image. The pixel used for automatic control was defined as the hottest pixel observed on temperature images acquired during an initial short-duration low-power

HIFU pulse (5 s, 10 W) performed at the beginning of the imaging session. The maximal temperature resulting from these tests never exceeded 40 °C.

The predefined heating pattern included a ramp time to reach the targeted temperature followed by a plateau. Mild hyperthermia protocols were performed for 5 min at 43; 44; 45 and 47 °C with ramp time of 1 min 24 s, 1 min 36 s, 1 min 36 s and 2 min, respectively. Thermal ablation protocols were performed for 1 min between 55 and 60 °C with a ramp time of 2 min. Thermometry data were re-processed offline with custom software written in MATLAB (Mathworks, ver. R2020a). In each pixel, the average temperature during the plateau of heating (either 25 images for 1 min of heating or 125 images for 5 min of heating) was computed. Then, these averaged temperature maps were filtered with a spatial low-pass filter which is the mean temperature of the surroundings voxels i.e. 9 voxels.

Bioluminescence imaging

BLI was performed using the Lumina LT imaging system (Perkin Elmer Inc., Boston, MA, USA) at the Vivoptic platform (Univ. Bordeaux, CNRS, INSERM, TBM-Core, UMS 3427, US 5, F-33000 Bordeaux). D-luciferin (2.9 mg; 100 µL PBS, Promega) or furimazin (20 µg; 100 µL PBS, Promega) were injected intraperitonealy for Fluc or Nluc imaging respectively. Bioluminescence acquisition (1 min, 4 x 4 binning) and photographs (100 ms) were taken 8 min after substrate injection. Data were analyzed with Living Image software (Perkin Elmer). Photon quantification was performed by drawing a region of interest (ROI) that encompassed the light-emitting region, and expressed as photons per second per centimeter squared and per steradian (photons/s/cm^2/sr) in the ROI. The BLI profile corresponds to the spatial distribution of the photon signals emitted by the tumor along the craniocaudal axis including the maximum intensity observed on the BLI image.

Histology

Excised tumors were embedded in matrix (OCT, CellPath, United Kingdom), frozen in liquid nitrogen-cooled isopentan and stored at – 80 °C. Frozen slices (10 µm) were then fixed in 4 % PFA (Deltamicroscopies, Mauressac, France) for 15 min. Hematoxylin Eosin Saffron (HES) staining was performed using ready-to-use hematoxylin solution (2 min, RAL Diagnostic, Martillac, France), erythrosine 239 solution (1 min; 10 g/L; RAL Diagnostics) and Saffron solution (15 s, 10 g/L in absolute ethanol, RAL Diagnostics). Tumor slides were mounted in DPX mounting medium (Leica, Wetzlar, Germany) and observed on an inverted microscope (Leica, Wetzlar, Germany) equipped with a Nikon camera.

Acknowledgements

We thank Sandrine Eimer (Bordeaux University) for help in histological slice analysis, Laetitia Medan (Bordeaux University) for animal breeding and care, and Stephanie Hoarau-Recco (Image-guided therapy, Pessac) for technical assistance for the thermoguide software. This work was supported by Labex TRAIL (ANR-10-LABEX-57) and France Life Imaging (ANR-11-INBS-006).

References

[1] D. Hanahan, L. M. Coussens, *Cancer Cell* **2012**, *21*, 309.
[2] S. Benavente, A. Sánchez-García, S. Naches, M. E. LLeonart, J. Lorente, *Front. Oncol.* **2020**, *10*, 582884.
[3] R. C. Ward, T. T. Healey, D. E. Dupuy, *Expert Rev. Med. Devices* **2013**, *10*, 225.
[4] T. P. Ryan, C. L. Brace, *Int. J. Hyperthermia* **2017**, *33*, 3.
[5] M. F. Meloni, J. Chiang, P. F. Laeseke, C. F. Dietrich, A. Sannino, M. Solbiati, E. Nocerino, C. L. Brace, F. T. Lee, *Int. J. Hyperth. Off. J. Eur. Soc. Hyperthermic Oncol. North Am. Hyperth. Group* **2017**, *33*, 15.

[6] E. Schena, P. Saccomandi, Y. Fong, *J. Funct. Biomater.* **2017**, *8*, 1110.
[7] P. Saccomandi, E. Schena, F. Giurazza, R. D. Vescovo, M. A. Caponero, L. Mortato, F. Panzera, R. L. Cazzato, F. R. Grasso, F. M. D. Matteo, et al., *Lasers Med. Sci.* **2014**, *29*, 607.
[8] K. Chen, S. Zhu, G. Xiang, X. Duan, J. He, G. Chen, *Saudi Pharm. J. SPJ* **2016**, *24*, 329.
[9] J. Palussière, V. Catena, J.-Y. Gaubert, X. Buy, T. de Baere, *Bull. Cancer (Paris)* **2017**, *104*, 417.
[10] M. Lepetit-Coiffé, H. Laumonier, O. Seror, B. Quesson, M.-B. Sesay, C. T. W. Moonen, N. Grenier, H. Trillaud, *Eur. Radiol.* **2010**, *20*, 193.
[11] Bour Pierre, Marquet Fabrice, Ozenne Valéry, Toupin Solenn, Dumont Erik, Aubry Jean-François, Lepetit-Coiffe Matthieu, Quesson Bruno, *Magn. Reson. Med.* **2017**, *78*, 1911.
[12] P. Bour, V. Ozenne, F. Marquet, B. D. de Senneville, E. Dumont, B. Quesson, *Int. J. Hyperthermia.* **2018**, 78, 1911.
[13] C. Sanchez, D. El Hajj Diab, V. Connord, P. Clerc, E. Meunier, B. Pipy, B. Payré, R. P. Tan, M. Gougeon, J. Carrey, et al., *ACS Nano* **2014**, *8*, 1350.
[14] P. Clerc, P. Jeanjean, N. Hallalli, M. Gougeon, B. Pipy, J. Carrey, D. Fourmy, V. Gigoux, *J. Controlled Release* **2018**, *270*, 120.
[15] E. Guisasola, L. Asín, L. Beola, J. M. de la Fuente, A. Baeza, M. Vallet-Regí, *ACS Appl. Mater. Interfaces* **2018**, *10*, 12518.
[16] R. Deckers, B. Quesson, J. Arsaut, S. Eimer, F. Couillaud, C. T. W. Moonen, *Proc. Natl. Acad. Sci. U. S. A.* **2009**, *106*, 1175.
[17] S. Roujol, M. Ries, B. Quesson, C. Moonen, B. D. de Senneville, *Magn. Reson. Med.* **2010**, *63*, 1080.
[18] M. J. Voogt, H. Trillaud, Y. S. Kim, W. P. Th. M. Mali, J. Barkhausen, L. W. Bartels, R. Deckers, N. Frulio, H. Rhim, H. K. Lim, et al., *Eur. Radiol.* **2012**, *22*, 411.
[19] J. W. Chang, B.-K. Min, B.-S. Kim, W. S. Chang, Y.-H. Lee, *Ultrasound Med. Biol.* **2015**, *41*, 124.
[20] W. S. Chang, H. H. Jung, E. J. Kweon, E. Zadicario, I. Rachmilevitch, J. W. Chang, *J. Neurol. Neurosurg. Psychiatry* **2015**, *86*, 257.
[21] B. Liberman, D. Gianfelice, Y. Inbar, A. Beck, T. Rabin, N. Shabshin, G. Chander, S. Hengst, R. Pfeffer, A. Chechick, et al., *Ann. Surg. Oncol.* **2009**, *16*, 140.
[22] D. Bonekamp, M. B. Wolf, M. C. Roethke, S. Pahernik, B. A. Hadaschik, G. Hatiboglu, T. H. Kuru, I. V. Popeneciu, J. L. Chin, M. Billia, et al., *Eur. Radiol.* **2019**, *29*, 299.
[23] J. L. Chin, M. Billia, J. Relle, M. C. Roethke, I. V. Popeneciu, T. H. Kuru, G. Hatiboglu, M. B. Mueller-Wolf, J. Motsch, C. Romagnoli, et al., *Eur. Urol.* **2016**, *70*, 447.
[24] S. Ghai, A. S. Louis, M. Van Vliet, U. Lindner, M. A. Haider, E. Hlasny, P. Spensieri, T. H. Van Der Kwast, S. A. McCluskey, W. Kucharczyk, et al., *AJR Am. J. Roentgenol.* **2015**, *205*, 174.
[25] D. Gianfelice, A. Khiat, M. Amara, A. Belblidia, Y. Boulanger, *Breast Cancer Res. Treat.* **2003**, *82*, 93.
[26] F. Wu, Z.-B. Wang, H. Zhu, W.-Z. Chen, J.-Z. Zou, J. Bai, K.-Q. Li, C.-B. Jin, F.-L. Xie, H.-B. Su, *Breast Cancer Res. Treat.* **2005**, *92*, 51.
[27] J. Lee, G. Farha, I. Poon, I. Karam, K. Higgins, S. Pichardo, K. Hynynen, D. Enepekides, *J. Ther. Ultrasound* **2016**, *4*, 12.
[28] D. El Hajj Diab, P. Clerc, N. Serhan, D. Fourmy, V. Gigoux, *Nanomaterials* **2018**, *8*, 468.
[29] N. R. Datta, S. G. Ordóñez, U. S. Gaipl, M. M. Paulides, H. Crezee, J. Gellermann, D. Marder, E. Puric, S. Bodis, *Cancer Treat. Rev.* **2015**, *41*, 742.

[30] A. Partanen, P. S. Yarmolenko, A. Viitala, S. Appanaboyina, D. Haemmerich, A. Ranjan, G. Jacobs, D. Woods, J. Enholm, B. J. Wood, et al., *Int. J. Hyperthermia* **2012**, *28*, 320.
[31] C. Bing, P. Patel, R. M. Staruch, S. Shaikh, J. Nofiele, M. W. Staruch, D. Szczepanski, N. S. Williams, T. Laetsch, R. Chopra, *Int. J. Hyperthermia* **2019**, *36*, 195.
[32] H. R. Kim, D. G. You, S.-J. Park, K.-S. Choi, W. Um, J.-H. Kim, J. H. Park, Y. Kim, *Mol. Pharm.* **2016**, *13*, 1528.
[33] N. Farr, Y.-N. Wang, S. D'Andrea, F. Starr, A. Partanen, K. M. Gravelle, J. S. McCune, L. J. Risler, S. G. Whang, A. Chang, et al., *Int. J. Hyperthermia* **2018**, 34, 284.
[34] C.-A. Cheng, W. Chen, L. Zhang, H. H. Wu, J. I. Zink, *J. Am. Chem. Soc.* **2019**, *141*, 17670.
[35] N. Frazier, A. Payne, J. de Bever, C. Dillon, A. Panda, N. Subrahmanyam, H. Ghandehari, *J. Controlled Release* **2016**, *241*, 186.
[36] E. Guilhon, P. Voisin, J. A. de Zwart, B. Quesson, R. Salomir, C. Maurange, V. Bouchaud, P. Smirnov, H. de Verneuil, A. Vekris, et al., *J. Gene Med.* **2003**, *5*, 333.
[37] O. F. Eker, B. Quesson, C. Rome, J. Arsaut, C. Deminière, C. T. Moonen, N. Grenier, F. Couillaud, *Radiology* **2011**, *258*, 496.
[38] N. Frazier, A. Payne, C. Dillon, N. Subrahmanyam, H. Ghandehari, *Nanomedicine Nanotechnol. Biol. Med.* **2017**, *13*, 1235.
[39] P.-Y. Fortin, M. Lepetit-Coiffé, C. Genevois, C. Debeissat, B. Quesson, C. T. W. Moonen, J. P. Konsman, F. Couillaud, *Oncotarget* **2015**, *6*, 23417.
[40] J. Ng, T. Dai, *Ann. Transl. Med.* **2016**, *4*, 118.
[41] A. Mehta, R. Oklu, R. A. Sheth, *Gastroenterol. Res. Pract.* **2016**, *2016*, 9251375.
[42] R. Slovak, J. M. Ludwig, S. N. Gettinger, R. S. Herbst, H. S. Kim, *J. Immunother. Cancer* **2017**, *5*, 78.
[43] B. Z. Fite, J. Wang, A. J. Kare, A. Ilovitsh, M. Chavez, T. Ilovitsh, N. Zhang, W. Chen, E. Robinson, H. Zhang, et al., *Sci. Rep.* **2021**, *11*, 927.
[44] L. Fass, *Mol. Oncol.* **2008**, *2*, 115.
[45] J. V. Frangioni, *J. Clin. Oncol.* **2008**, *26*, 4012.
[46] M. L. White, Y. Zhang, F. Yu, N. Shonka, M. R. Aizenberg, P. Adapa, S. A. J. Kazmi, *PLoS ONE* **2019**, *14*, e0213905.
[47] J. P. B. O'Connor, *Semin. Cell Dev. Biol.* **2017**, *64*, 48.
[48] M. W. Dewhirst, D. E. Thrall, G. Palmer, T. Schroeder, Z. Vujaskovic, H. Cecil Charles, J. Macfall, T. Wong, *Int. J. Hyperth. Off. J. Eur. Soc. Hyperthermic Oncol. North Am. Hyperth. Group* **2010**, *26*, 283.
[49] C. E. O'Connell-Rodwell, M. A. Mackanos, D. Simanovskii, Y.-A. Cao, M. H. Bachmann, H. A. Schwettman, C. H. Contag, *J. Biomed. Opt.* **2008**, *13*, 030501.
[50] N. Alsawaftah, A. Farooq, S. Dhou, A. F. Majdalawieh, *IEEE Rev. Biomed. Eng.* **2021**, *14*, 307.
[51] O. Sandre, C. Genevois, E. Garaio, L. Adumeau, S. Mornet, F. Couillaud, *Genes* **2017**, *8*, 61.
[52] P.-Y. Fortin, C. Genevois, M. Chapolard, T. Santalucía, A. M. Planas, F. Couillaud, *Biomed. Opt. Express* **2014**, *5*, 457.
[53] J. E. Kennedy, *Nat. Rev. Cancer* **2005**, *5*, 321.
[54] R. Salomir, F. C. Vimeux, J. A. de Zwart, N. Grenier, C. T. W. Moonen, *Magn. Reson. Med.* **2000**, *43*, 342.
[55] M. O. Köhler, C. Mougenot, B. Quesson, J. Enholm, B. L. Bail, C. Laurent, C. T. W. Moonen, G. J. Ehnholm, *Med. Phys.* **2009**, *36*, 3521.
[56] J. K. Enholm, M. O. Kohler, B. Quesson, C. Mougenot, C. T. W. Moonen, S. D. Sokka, *IEEE Trans. Biomed. Eng.* **2010**, *57*, 103.
[57] K. Pinel, C. Genevois, C. Debeissat, F. Couillaud, *Sci. Rep.* **2018**, *8*, 1.

[58] P. C. Lyon, L. F. Griffiths, J. Lee, D. Chung, R. Carlisle, F. Wu, M. R. Middleton, F. V. Gleeson, C. C. Coussios, *J. Ther. Ultrasound* **2017**, *5*, 28.
[59] X. de la Rosa, T. Santalucía, P.-Y. Fortin, J. Purroy, M. Calvo, A. Salas-Perdomo, C. Justicia, F. Couillaud, A. M. Planas, *Eur. J. Nucl. Med. Mol. Imaging* **2013**, *40*, 426.
[60] C. Germain-Genevois, O. Garandeau, F. Couillaud, *Mol. Imaging Biol.* **2016**, *18*, 62.
[61] M. D. Ryan, J. Drew, *EMBO J.* **1994**, *13*, 928.
[62] L. Adumeau, C. Genevois, L. Roudier, C. Schatz, F. Couillaud, S. Mornet, *Biochim. Biophys. Acta BBA - Gen. Subj.* **2017**, *1861*, 1587.
[63] M. Rezaei, K. Khoshgard, M. Mousavi, *J. Med. Signals Sens.* **2017**, *7*, 178.
[64] Y. Ishihara, A. Calderon, H. Watanabe, K. Okamoto, Y. Suzuki, K. Kuroda, Y. Suzuki, *Magn. Reson. Med.* **1995**, *34*, 814.
[65] J. D. Poorter, C. D. Wagter, Y. D. Deene, C. Thomsen, F. Ståhlberg, E. Achten, *Magn. Reson. Med.* **1995**, *33*, 74.
[66] R. T. D. Peters, R. S. Hinks, R. M. Henkelman, *Magn. Reson. Med.* **1998**, *40*, 454.

Supporting Information

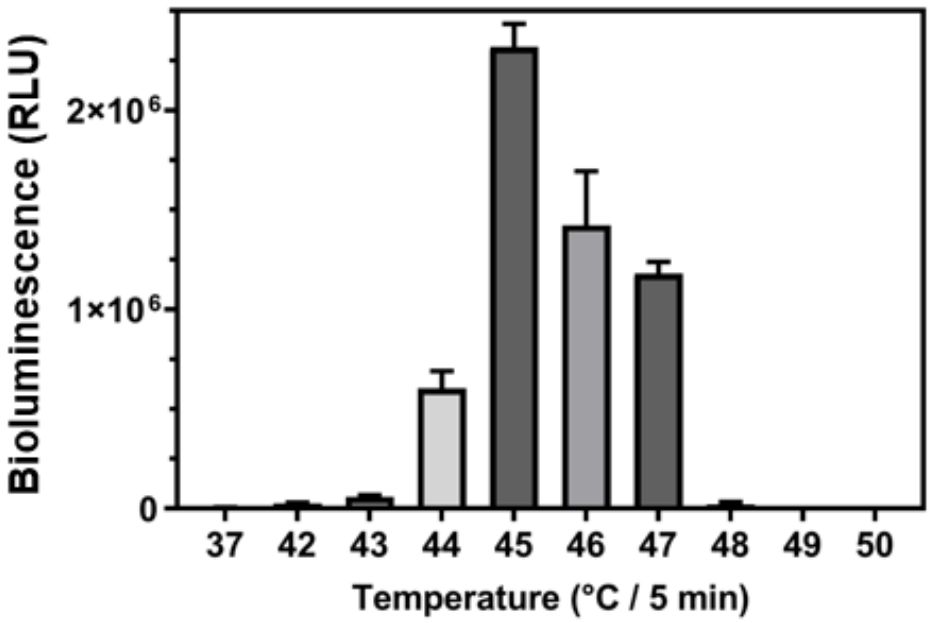

Figure S1. *In vi*tro characterization of RM1-Hsp70-Fluc cells response after water bath heating. Graph shows Fluc activity for 10^5 cells at different heating conditions for 5 min from 42 to 48 °C. Bars indicate means, vertical lines indicates standard deviations (N = 3). Cells (10^5 cells per well) were first incubated for 24 hours at 37 °C, then heated by using a water bath. After heat shock, cells were returned to 37 °C in a 5 % CO_2 incubator for 6 hours. Fluc activities were assayed with the Luciferase Assay System (Promega) and photons counted with a luminometer (Lumat 9501, Berthold Technology, Bad Wildbad, Germany).

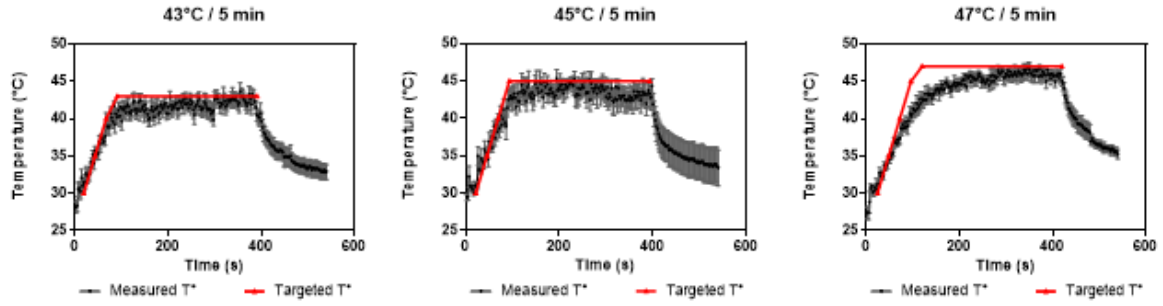

Figure S2. Temperature profiles of tumor mild hyperthermia treatments induced by MRgHIFU. Means of measured temperature ± SEM (grey curves) and feedback temperature (red curves) for each heating condition: 43°C (N = 7); 45°C (N = 6) and 47 °C (N = 6) for 5 min.

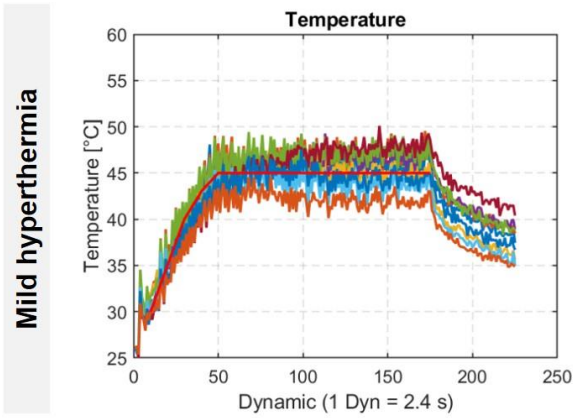

Voxel	Mean temperature °C
Average	45.44
1	47.00
2	46.01
3	46.89
4	45.14
5	46.33
6	44.00
7	46.85
8	44.56
9	42.19

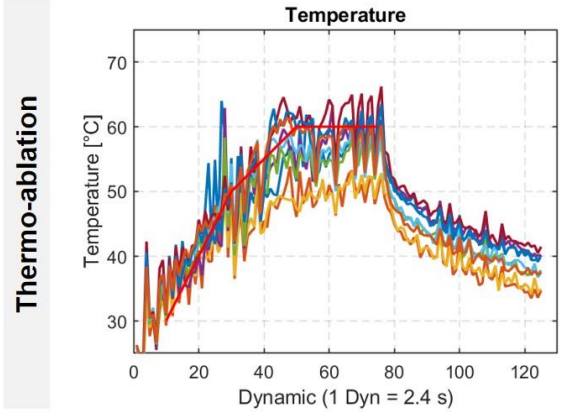

Voxel	Mean temperature °C
Average	55.64
1	54.61
2	55.83
3	49.95
4	49.94
5	57.07
6	55.75
7	61.06
8	58.80
9	57.71

Figure S3. Examples of voxel temperature analysis during tumor mild hyperthermia and tumor thermo-ablation. The temperature of the reference voxel and the 8 surrounding voxels were analyzed to determine the average measured temperature on the plateau within the tumor.

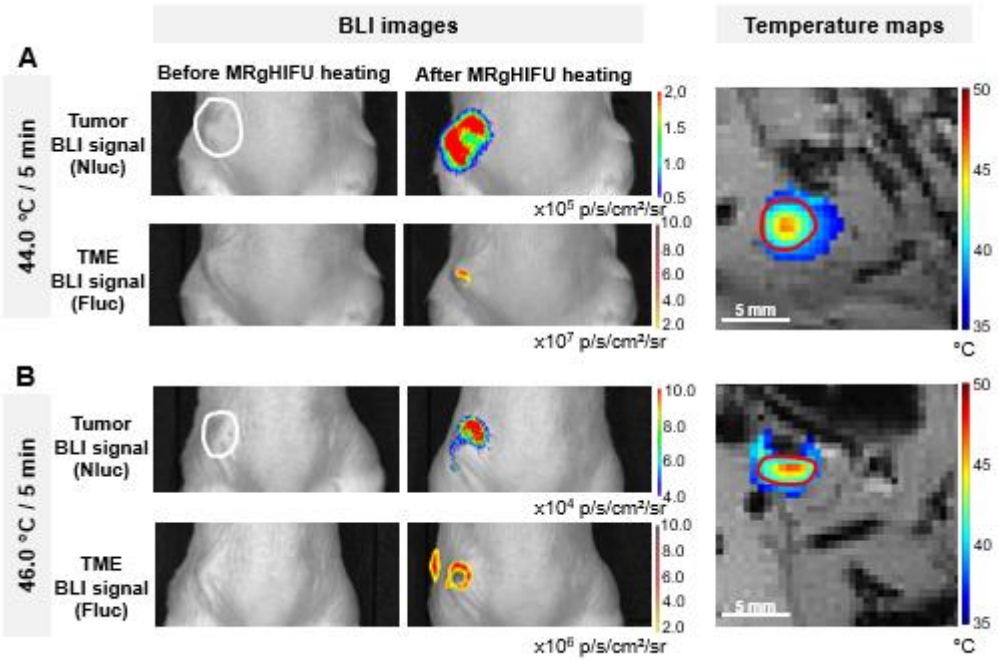

Figure S4. Changes in BLI signal after mild hyperthermia in tumor and TME induced by MRgHIFU heating. Transgenic mice with thermo-inducible Fluc expression (Hsp-Fluc) bearing RM1 tumors with thermo-inducible expression of Nluc (RM1-Hsp70-Nluc). BLI images of tumor and TME, before and after MRgHIFU heating and temperature map of a mouse treated at 46.8 °C for 5 min. Fluc and Nluc BLI images after MRgHIFU heating were captured at 6 and 24 h, respectively. The white line in BLI images delimits the tumor edge. Temperature maps represent the average temperature of MRgHIFU heating and the mean temperature of the surroundings voxels. The red line in the temperature map delimits tumor edge defined on MRI images prior to heating.

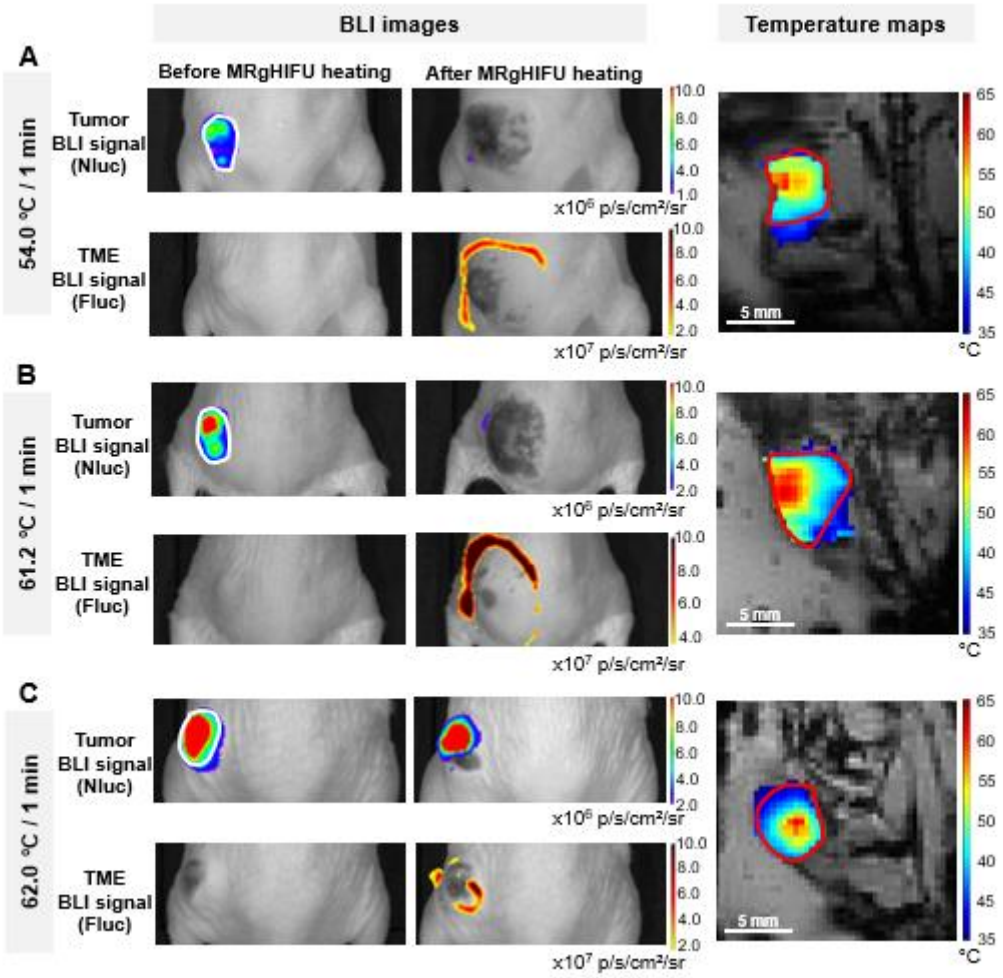

Figure S5. Tumor thermal ablation by MRgHIFU heating and BLI assessment TME activation by BLI. Transgenic mice with thermo-inducible Fluc expression (Hsp-Fluc) bearing RM1 tumors with constitutive expression of Nluc (RM1-CMV-Nluc). BLI images before and after MRgHIFU treatment and temperature maps of 2 mice treated at 55.5 °C / 1 min (**A**) and 57 °C / 1 min (**B**). The BLI images after MRgHIFU heating of the TME and the tumor were captured 6 and 24 hours respectively after the heating treatment. The white line in BLI images delimits the tumor edge. Temperature maps represent the average temperature of MRgHIFU heating and the mean temperature of the surroundings voxels. The red line in the temperature map delimits tumor edge defined on MRI images prior to heating.